Silvestri *et al.*
Progress in Earth and Planetary Science (2022) 9:45
https://doi.org/10.1186/s40645-022-00490-7

Progress in Earth and Planetary Science

COMMENT

Open Access

Comment on "Soil salinity assessment by using near-infrared channel and Vegetation Soil Salinity Index derived from Landsat 8 OLI data: a case study in the Tra Vinh Province, Mekong Delta, Vietnam" by Kim-Anh Nguyen, Yuei-An Liou, Ha-Phuong Tran, Phi-Phung Hoang and Thanh-Hung Nguyen

Sonia Silvestri[1*], Diep Ngoc Nguyen[2,3] and Emilia Chiapponi[1]

Abstract

Nguyen et al. (Prog Earth Planet Sci 7:1, 2020. https://doi.org/10.1186/s40645-019-0311-0) suggest that Landsat 8 OLI can be used to map and monitor soil salinity in the coastal zone of the Mekong River Delta. The authors use empirical correlations between the near-infrared (NIR) band, or vegetation indexes containing the NIR band, and soil salinity. We show that within the coastal portion of the Mekong Delta, extensively ponded due to widespread shrimp farming, about 90% of Landsat 8 pixels are fully or partially covered by water. We then find that, due to strong NIR radiation absorption, NIR reflectance from ponded pixels decreases linearly with increasing water percentage cover, while no significant correlation is found between reflectance and soil salinity. Through detailed new analyses, we conclude that NIR reflectance attenuation cannot be ascribed to vegetation stress caused by soil salinity, but rather to the presence of water ponds. We also show that a similar behavior exists in ponded freshwater inland areas, confirming that the NIR absorption exerted by water is independent of salinity.

Keywords: Soil salinity, Mekong River Delta, Coastal areas, Wetlands, Landsat 8 OLI, Google Satellite, Near-infrared reflectance reduction, Water absorption, Mixed pixels

1 Introduction

Nguyen et al. (2020) suggest that soil salinity can be monitored using Landsat 8 OLI (L8 hereafter) in the coastal zone of the Mekong River Delta. The study suggests an inverse exponential correlation between the near-infrared (NIR) band (i.e., L8 band-5) and the electrical conductivity ($EC_{1:5}$) (i.e., determined using a conductivity probe on a mix of 1 part soil with 5 parts deionized water) determined at several points within their study site (Tra Vinh Province, Fig. 6 plot d of Nguyen et al. 2020). Significant correlations between vegetation indexes that include the NIR band and soil $EC_{1:5}$ are also highlighted in the study (see Fig. 8 plots SI4, NDSI, NDVI, SAVI and VSSI of Nguyen et al. 2020). The authors underline the good performance of the Vegetation Soil Salinity Index (proposed by Dehni

*Correspondence: sonia.silvestri5@unibo.it

[1] Department of Biological, Geological and Environmental Sciences, University of Bologna, P.za Porta S. Donato 1, 40126 Bologna, Italy
Full list of author information is available at the end of the article

and Lounis (2012) as VSSI = 2 × green − 5 × (red + NIR), where "green" and "red" are the L8 band-3 and the L8 band-4, respectively).

The Tra Vinh Province covers a large territory that includes inner agricultural lands as well as a coastal wetland zone, characterized by an extensive presence of ponds for shrimp farming (Wassmann et al. 2019). Focusing exclusively on the latter, we will show in this comment article that (1) L8 spatial resolution is not suitable to distinguish between ponded and non-ponded areas; therefore, (2) the decreased NIR reflectance ascribed to increased soil salinity is instead due to the presence of water in L8 mixed pixels. Finally, (3) we show that NIR reflectance is equally reduced independently of whether the water ponding area is saltwater or freshwater.

Salinity affects vegetation development and its health status. Some vegetation species, as halophytes, can grow on salt marsh salted soil because they developed specific adaptation measures (Silvestri and Marani 2004). Mangroves are also highly tolerant to salinity, thanks to a range of adaptations (Parida and Jha 2010). However, in areas other than coastal saline wetlands, salt is toxic to vegetation and affects the development of natural vegetation as well as crop production (Montanarella et al. 2015; Vargas et al. 2018). Hence, in these cases, remote sensing can be used to detect the stress that salt produces on plants, causing lower photosynthetic activity (Tilley et al. 2007; Zhang et al. 2015; Scudiero et al. 2015). Specifically, decreased near-infrared (NIR) reflectance is observed when vegetation is subjected to salinity stress (Wang et al. 2002; Tilley et al. 2007; Zhang et al. 2011). L8 has been used for this purpose in other studies (Scudiero et al. 2015; Gorji et al. 2020). However, factors other than salinity stress may be responsible for a reduction in NIR reflectance, as the presence of water around or underneath the vegetation, a well-known effect in wetlands (Silva et al. 2008; Hestir et al. 2008; Adam et al. 2010). Therefore, the conclusion that a reduction in the NIR reflectance is due to vegetation stress caused by increased salinity must be carefully tested in coastal wetlands, and the influence of water absorption must be accounted for (Dekker et al. 2002).

Here, we focus on the same L8 OLI image analyzed by Nguyen et al. (2020), acquired on February 14, 2017, and available in USGS EarthExplorer. We selected the Collection-2 Level-2 product (see detailed characteristics in Additional file 1: Table S1), which is geometrically, radiometrically and atmospherically corrected to surface reflectance by USGS (2022). We masked the areas covered by clouds.

2 Main text

2.1 Landsat 8 OLI spatial resolution is not adequate to study soil salinity in the ponded coastal zone of the Mekong River Delta

Wetlands are characterized by partly emerged and submerged areas. The coastal portion of the Mekong River Delta is characterized by an almost continuous presence of artificial ponds, mainly used for shrimp farming (Fig. 1). Ponds are surrounded by embankments with little streets, small villages, bare soil as well as vegetated areas. In order to identify emerged vegetation and study its health status, the spatial resolution allowing pixels to be mostly "pure" (i.e., either exclusively composed of fully emerged or fully submerged areas) should first be determined. Too coarse resolution, in fact, gives a large percentage of mixed pixels, i.e., pixels comprising both emerged and flooded areas, with a reflectance that is intermediate between those from both categories. To understand if Landsat data can be used to discriminate ponded vs non-ponded surfaces, we must determine the probability that pixels contain portions of standing waters. We can perform such analysis by generating a grid with cells of 30 m × 30 m, overlaying on L8 pixels, and by counting the number of cells that fully fall on water ponds, land and mixed water/land areas. Since the coastal ponded area within the Tra Vinh Province is very large (more than 275 km^2, see Fig. 1), we performed these analyses by generating 20 grids of 10 × 10 cells (of 30 m × 30 m each) distributed across the ponded area. Twelve grids were created around the sampling points described in Nguyen et al. (2020; points with IDs 30–41 listed in Table 4), while other eight grids were randomly generated in QGIS across the remaining ponded area (Fig. 1). The detection of the grid cells falling on water ponds or on emerged land was determined with a visual inspection method in QGIS using Google Earth satellite as base image. Google Earth is the most accurate high-resolution virtual globe currently available and covers almost the entire land surface of the Earth (Yu and Gong 2012; Guo et al. 2020). It integrates aerial photographs with medium to high spatial resolution satellite images mainly collected by WorldView-1/2/3, GeoEye-1, Airbus' Pleiades, QuickBird, Landsat and SPOT5. Such integration allows the operator to zoom to around 0.3–0.5 m resolution (see Additional file 1: Table S2 for details) depending on the availability of satellite images in different locations of the world. Therefore, the advantage of using Google Earth is that it provides a recent cloud-free base image with an extremely high spatial resolution that allows the operator to clearly detect water ponds and land. The horizontal accuracy of Google Earth varies for different locations of the world and is strongly affected by topography, being lower on mountainous

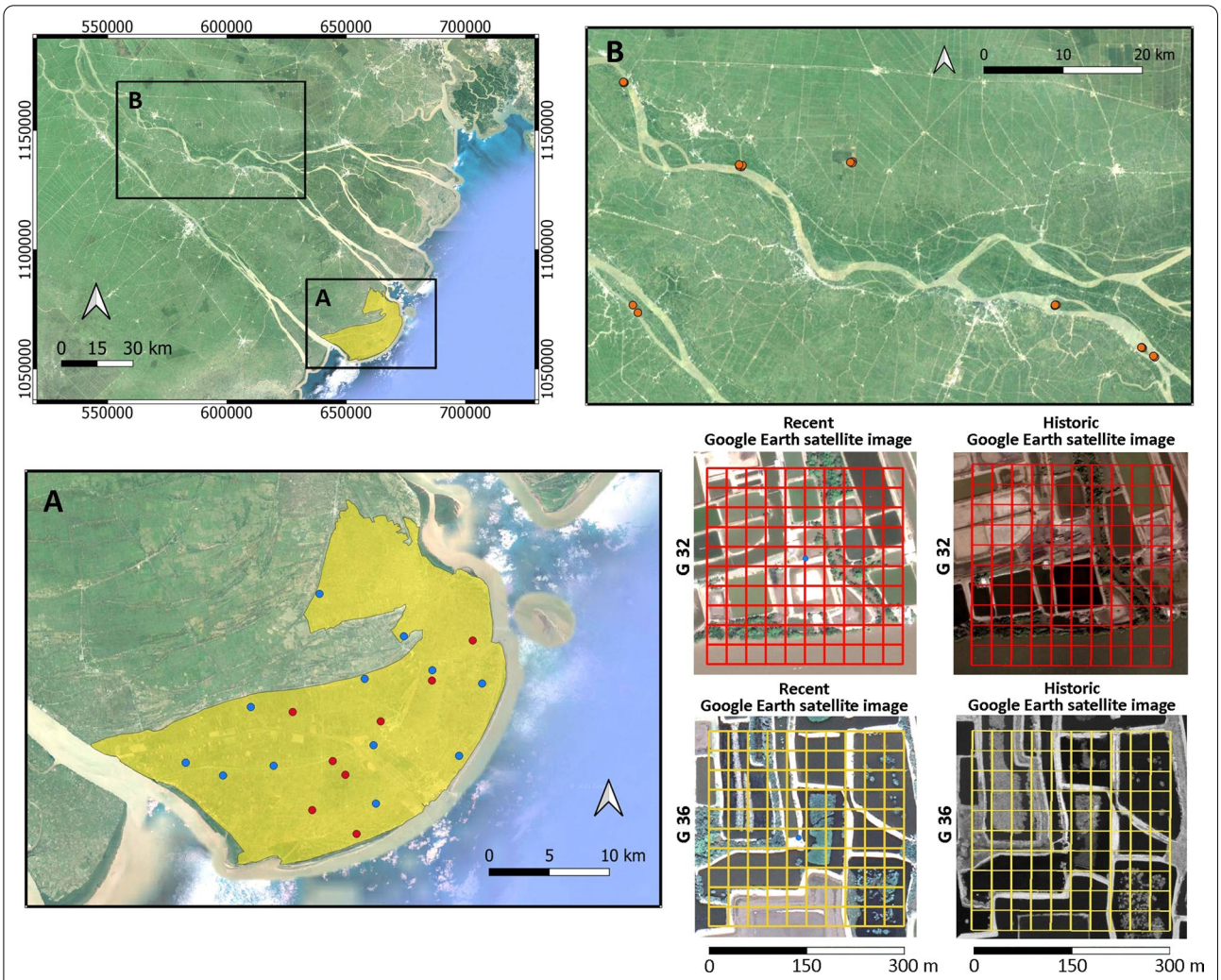

Fig. 1 The upper left panel shows the study area: the yellow polygon indicates the coastal zone with ponds used for shrimp farming, which is magnified in the **A** panel; the **B** panel shows the freshwater area. Blue points in the **A** panel indicate the location of the grids created around the twelve sampling points provided by Nguyen et al. (2020); red points in the **A** panel indicate the location of the eight additional grids randomly generated; orange points in the **B** panel indicate the location of the grids created on freshwater ponds. The images of the grids of 10 × 10 cells (of 30 m × 30 m each) in the bottom right of the figure correspond to the grids created around point with ID 32 and around point with ID 36 overlaid on the most recent and on the historic Google Earth satellite images (see Table 1 for the exact dates of the images). Coordinate reference system: WGS84 UTM Zone 48. Maps were produced in QGIS and Google Earth Pro using Google Earth satellite images

terrain and higher on plains. Several studies have shown that on plains and lowlands the absolute positioning accuracy generally varies between 0.1 and 5.0 m (Benker et al. 2011; Paredes-Hernandez et al. 2013; Goudarzi and Landry Jr 2017; Guo et al. 2020). The disadvantage is that Google Earth is a collage of images collected very recently but in different periods, and some land-use changes may have occurred since 2017, when the L8 image used in this study was acquired. Some differences may also be due to seasonal variations or differences in water levels. Moreover, given the typically high humidity of the Mekong delta, some areas are still covered by clouds. Therefore, to further verify the method, we also used Google Earth Pro to explore the database of available images, including those collected before February 2017, by overlaying the same 20 grids generated in QGIS. Figure 1 shows an example of two generated grids, while Table 1 shows the number of cells that, within each grid of 10 × 10 cells, fully fall within water ponds, land or on mixed surfaces using the recent Google Earth image as well as cloud-free images collected before February 2017. The table includes the dates of the analyzed images. We notice that, on average, more than 86% of the cells contain both water and emerged areas, and almost 4% fall on

Table 1 Number of grid cells fully falling on water, land or mixed water/land

	ID	G30	G31	G32	G33	G34	G35	G36	G37	G38	G39	G40	G41	R1	R2	R3	R4	R5	R6	R7	R8	Mean %
Recent images	Water	0	2	15	0	5	2	6	2	1	5	3	0	1	0	13	2	3	6	5	4	**3.75**
	Land	12	7	0	0	3	2	0	34	25	17	10	2	6	28	18	5	1	5	17	2	**9.7**
	Mix	88	91	85	100	92	96	94	64	74	78	87	98	93	72	69	93	96	89	78	94	**86.55**
	Image date	M18	M18	F18	D19	M18	D19	F18	D19	F18	D19	D19	F18	D19	D19	D19	D19	D19	D19	M18	D19	
Historical images	Water	0	0	17	0	5	1	6	4	3	4	2	0	0	0	11	0	5	6	9	3	**3.8**
	Land	17	7	14	0	1	4	3	32	33	0	6	0	1	26	14	4	0	5	14	3	**9.2**
	Mix	83	93	69	100	94	95	91	64	64	96	92	100	99	74	75	96	95	89	77	94	**87**
	Image date	J15	A14	J15	A14	A14	J15	M11	J15	J15	A14	A14	A14	A14	J15	J06	A14	A14	A14	J15	A14	

Cells sum to 100 for each grid. G30 to G41 are grids created around the corresponding field points of Nguyen et al. (2020) (see IDs of Table 4). R1 to R8 are grids created around random points falling within the coastal ponded zone. Google Earth satellite images are used as base images. The first part of the table is produced using the recent base images (collected on December 2019, March 2018 and February 2018, reported in the table as D19, M18 and F18, respectively). The second part is produced using historical cloud-free base images collected before February 14, 2017 (collected on January 2015, August 2014, March 2011 and January 2006, reported in the table as J15, A14, M11 and J06, respectively)

water ponds, confirming that the large majority of L8 pixels are affected by the presence of water.

Pixels that fully or partially fall on water bodies are affected by the water ability to absorb incident energy in the infrared portion of the electromagnetic spectrum, attenuating the reflected NIR signal (see Dekker et al. 2002) and therefore interfering with any possible signal attenuation linked to vegetation stress. Our results indicate that in the ponded coastal area of the Tra Vinh Province, about 90% of the Landsat pixels are affected by the presence of water and should be masked to avoid the NIR reflectance attenuation exerted by water. Only the remaining 10% can be used to study a possible correlation between soil salinity and NIR reflectance, using salinity field measurements performed exclusively within pixels that fully fall on emerged land. This method would provide a map with more than 90% of masked pixels. Therefore, we conclude that L8 spatial resolution is not suitable for this purpose in the ponded coastal area of the Tra Vinh Province. High spatial resolution satellites, such as WorldView-3 or Planet, would provide a much larger number of pixels falling on emerged land, allowing a more effective analysis.

2.2 The presence of ponds influences the NIR signal (and the vegetation indexes containing NIR), masking possible relations with soil $EC_{1:5}$ in the coastal area of the Tra Vinh Province

We selected twelve L8 pixels corresponding to the field measurement points described in Nguyen et al. (2020) across the coastal area (points with IDs 30–41 listed in Table 4). The location of the twelve points can be seen in Additional file 1: Fig. S1. We notice that the points fall on embankments surrounded by ponds and channels and that eleven out of the twelve L8 OLI pixels corresponding to the sampling points fall on mixed water/land surfaces (Additional file 1: Fig. S1). We notice that two points (point G30 and point G41) fall at the edge between land and water, and point G40 falls on water, even though very close to the embankment. This may be due to a low precision of the Global Navigation Satellite System (GNSS) receiver used by the authors or to a low absolute positioning accuracy of the Google Earth images as discussed in the previous chapter. Nevertheless, we underline that an error of a few meters in the relative positioning of GNSS points is small with respect to the size of the L8 pixels themselves. We notice that in all cases, pixels and their nearest neighbors contain a very high proportion of water. In order to quantify the water percentage cover within each selected pixel, we generated 100 regularly spaced points (see Additional file 1: Fig. S2). As we did for the analysis described at paragraph 2.1, we used recent and historical Google Earth satellite images (see Table 1 for image dates) to visually determine the number of points falling on water ponds (Additional file 1: Fig. S2). This number is the best available proxy of actual water percentage cover. Figure 2a shows that there is a significant linear correlation (P value < 0.01) between the water percentage cover and the L8 NIR band reflectance: Reflectance decreases with increasing water percentage cover, confirming that shrimp farming ponds interfere with the reflectance signal, by absorbing near-infrared electromagnetic energy. This correlation is slightly stronger if we consider the values of water percentage cover determined using historical images in Google Earth. No significant correlation could be found between $EC_{1:5}$ and the L8 NIR reflectance (Fig. 2). We also performed a multiple regression of L8 NIR reflectance on $EC_{1:5}$ and water percentage cover as independent variables. We find that L8 NIR reflectance variability is almost totally explained by water percentage cover, while the correlation with EC1:5 is not significant (P value > 0.05). A similar behavior is observed when

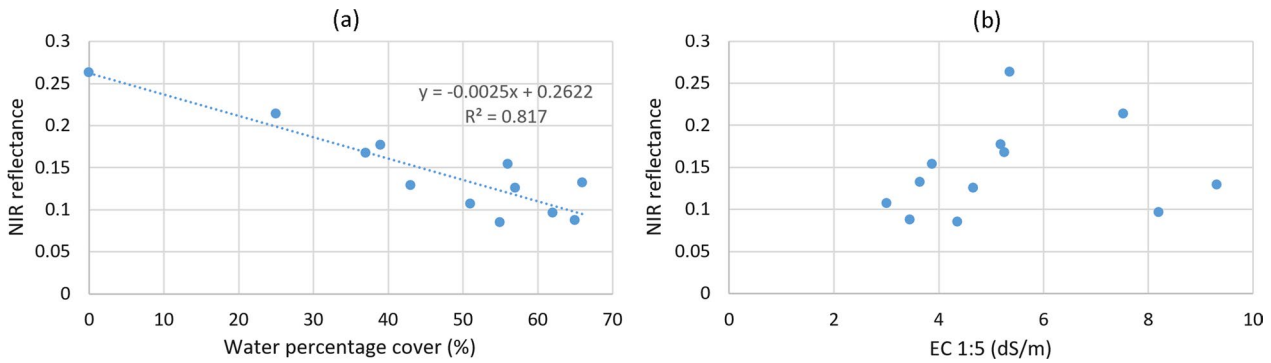

Fig. 2 Relationship of the L8 NIR reflectance of the G30–G41 pixels with **a** the water percentage cover and **b** the $EC_{1:5}$ provided by Nguyen et al. (2020)

considering the VSSI as a dependent variable instead of the NIR reflectance.

2.3 The presence of ponds reduces NIR reflectance whether they contain saltwater or freshwater

In order to explore the possible influence of salt on the previous analysis, we compared the effect of the water presence on the NIR reflectance in freshwater and saline ponded environments. Therefore, we randomly selected 20 pixels falling on freshwater ponds in the inner Mekong River Delta, at a distance higher than 60 km from the mouth (Fig. 1), so that the ponds are not affected by salinity (Eslami et al. 2019; Wassmann et al. 2019). As for the coastal saline area, in order to match the 20 observations selected in the freshwater area, to the original 12 pixels corresponding to the field observations performed by Nguyen et al. (2020), we added 8 pixels randomly selected within the grids used to determine if the L8 spatial resolution were adequate (Fig. 1). We generated 100 points regularly spaced within all the created pixels. Figure 3 shows that in (a) saltwater ponded areas as well as in (b) freshwater ponded areas, there is a significant linear correlation (P value < 0.01) between water percentage cover and reflectance of the L8 NIR band. Similarly, Fig. 3 shows that there is a significant linear correlation (P value < 0.01) also between water percentage cover and the VSSI for (c) saltwater and (d) freshwater ponded areas. Our results confirm that NIR reflectance is gradually reduced by an increasing water surface, in both salted and freshwater environments. This result confirms that salinity does not influence the absorption of the incident energy exerted by water.

3 Conclusions

Nguyen et al. (2020) has the merit of exploring the use of L8 OLI to study the influence of salinity on vegetation in the Mekong River Delta. Even though the L8 spatial resolution is suitable to perform the analysis on the inner agriculture land of the Tra Vinh Province considered by the authors, we show that the method cannot be applied to the coastal area where shrimp farming ponds are widely present. We have shown that L8 spatial resolution is not suitable to distinguish between ponded and non-ponded areas in the coastal portion of the Tra Vinh Province, because about 90% of the L8 pixels fully or partially fall on ponds and canals. We have also shown that the attenuation of the NIR reflectance is primarily due to the water presence and decreases linearly with increasing water percentage cover, while no significant correlation between soil salinity and NIR reflectance could be found.

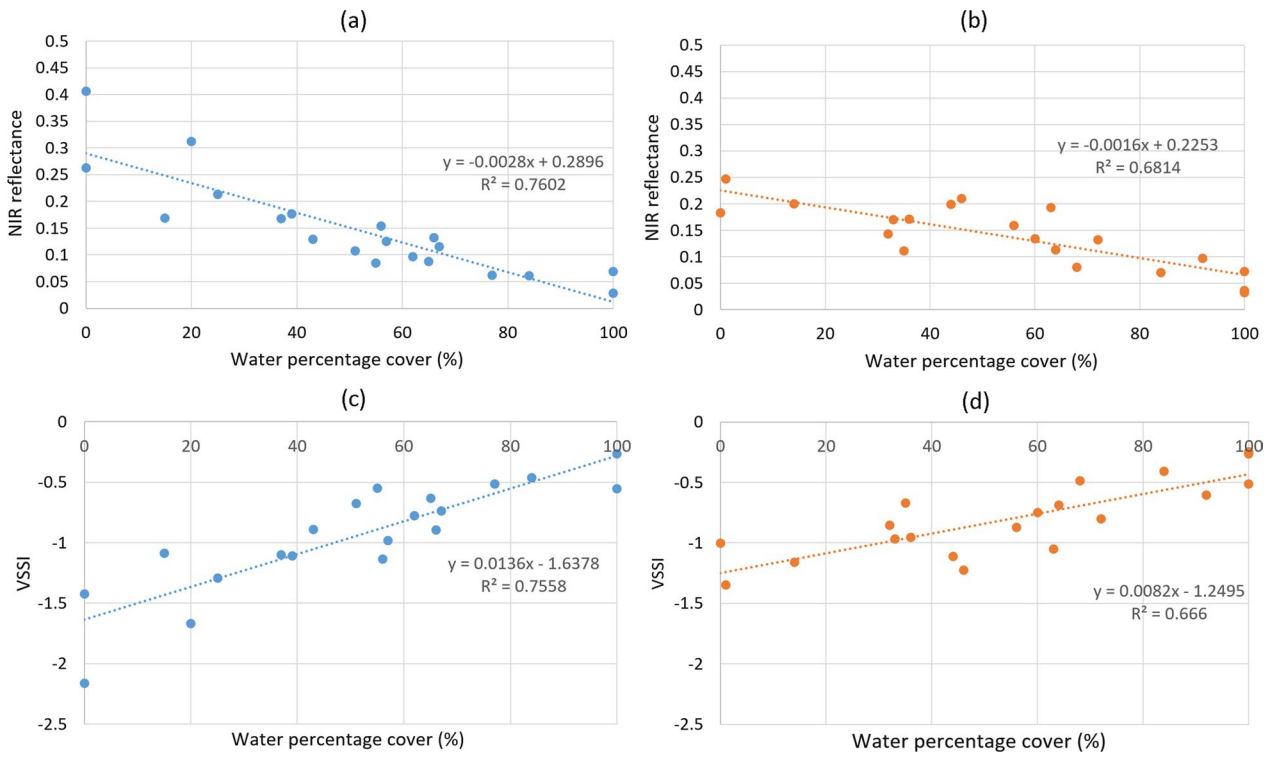

Fig. 3 Relationship of the L8 NIR reflectance with the water percentage cover in **a** the coastal area and **b** in the freshwater area (plot A and plot B of Fig. 1, respectively). Relationship of the VSSI with the water percentage cover (**c**) in the coastal area and **d** in the freshwater area

The attenuation of the NIR reflectance due to the presence of water ponds is similar in the coastal saline area and in the inner freshwater area.

Supplementary Information

The online version contains supplementary material available at https://doi.org/10.1186/s40645-022-00490-7.

Additional file 1. Supplementary figures and tables.

Acknowledgements
Diep Nguyen Ngoc and the collaboration among the authors were supported by the European Commission under the Erasmus Mundus Joint Master Degree Programme in Water and Coastal Management [Grant Number 586596-EPP-1-2017-1-IT-EPPKA1-JMDMOB]. The authors would like to acknowledge the anonymous reviewers of this article who gave an important contribution to improve it.

Author contributions
SS proposed the topic, conceived and designed the study, carried out the experimental study, analyzed the data and interpreted the results, and wrote the manuscript. DNN and EC collaborated in analyzing the data and helped in their interpretation. All authors read and approved the final manuscript. Sonia Silvestri is a Senior Assistant Professor at the University of Bologna (Italy), Department of Biological, Geological, and Environmental Sciences. She holds a position as an Adjunct Associate Professor at Duke University, USA (Division of Earth & Ocean Sciences, Nicholas School of the Environment). She is also a fellow of the Venice International University, Venice, Italy. Her research focuses on active and passive remote sensing applied to vegetation mapping, soil studies, hydrology, tidal environments morphology, water quality in coastal environments; hyperspectral imagery analysis; peatland detection through remote sensing and airborne geophysical methods; ecology of wetlands; and wetlands ecogeomorphology. Diep Nguyen Ngoc holds a research contract at the Department of Environmental Sciences, Informatics and Statistics, Ca' Foscari University (Italy), in collaboration with the Risk Assessment and Adaptation Strategies Division, Euro-Mediterranean Center on Climate Change. She is currently working at a project that aims at assessing the impacts of multi-risks induced by multiple climatic stressors in the Metropolitan city of Venice. Emilia Chiapponi is a Ph.D. student at the University of Bologna (Italy), Department of Biological, Geological, and Environmental Sciences. She is currently working on greenhouse gas emissions and carbon balance along a salinity gradient in coastal wetlands. All authors read and approved the final manuscript.

Funding
European Commission under the Erasmus Mundus Joint Master Degree Programme in Water and Coastal Management [Grant Number 586596-EPP-1-2017-1-IT-EPPKA1-JMDMOB].

Availability of data and materials
The dataset supporting the conclusions of this article is available in the ZENODO repository at: https://zenodo.org/deposit/5853516 with https://doi.org/10.5281/zenodo.5853516.

Declarations

Ethical approval
This article does not contain any studies with human participant or animals performed by any of the authors.

Competing interests
The authors declare that they have no competing interests.

Author details
[1]Department of Biological, Geological and Environmental Sciences, University of Bologna, P.za Porta S. Donato 1, 40126 Bologna, Italy. [2]Department of Environmental Sciences, Informatics and Statistics, Ca' Foscari University of Venice, Via Torino 155, 30172 Mestre, VE, Italy. [3]Risk Assessment and Adaptation Strategies Division, Euro-Mediterranean Center on Climate Change, Via della Libertà, 12, 30175 Venice, VE, Italy.

Received: 27 January 2022 Accepted: 17 May 2022
Published online: 02 September 2022

References

Adam E, Mutanga O, Rugege D (2010) Multispectral and hyperspectral remote sensing for identification and mapping of wetland vegetation: a review. Wetlands Ecol Manag 18(3):281–296
Benker SC, Langford RP, Pavlis TL (2011) Positional accuracy of the Google Earth terrain model derived from stratigraphic unconformities in the Big Bend region, Texas, USA. Geocarto Int 26(4):291–303
Dehni A, Lounis M (2012) Remote sensing techniques for salt affected soil mapping: application to the Oran region of Algeria. Procedia Eng 33:188–198
Dekker AG, Brando VE, Anstee JM, Pinnel N, Kutser T, Hoogenboom EJ, Peters S, Pasterkamp R, Vos R, Olbert C, Malthus TJ (2002) Imaging spectrometry of water. In: van der Meer FD, De Jong SM (eds) Imaging spectrometry. Springer, Dordrecht, pp 307–359. https://doi.org/10.1007/978-0-306-47578-8_11
Eslami S, Hoekstra P, Trung NN, Kantoush SA, Van Binh D, Quang TT, van der Vegt M (2019) Tidal amplification and salt intrusion in the Mekong Delta driven by anthropogenic sediment starvation. Sci Rep 9(1):1–10
Gorji T, Yildirim A, Hamzehpour N, Tanik A, Sertel E (2020) Soil salinity analysis of Urmia Lake Basin using Landsat-8 OLI and Sentinel-2A based spectral indices and electrical conductivity measurements. Ecol Indic 112:106173
Goudarzi MA, Landry R Jr (2017) Assessing horizontal positional accuracy of Google Earth imagery in the city of Montreal, Canada. Geod Cartogr 43(2):56–65
Guo J, Zhang JX, Zhao HT, Li C, Zhou J, Tu HJ, Zhao Y (2020) Horizontal accuracy assessment of Google Earth data over typical regions of Asia. Int Arch Photogramm Remote Sens Spatial Inf Sci 43:1333–1338
Hestir EL, Khanna S, Andrew ME, Santos MJ, Viers JH, Greenberg JA, Rajapakse SS, Ustin SL (2008) Identification of invasive vegetation using hyperspectral remote sensing in the California Delta ecosystem. Remote Sens Environ 112(11):4034–4047
Montanarella L, Badraoui M, Chude V, Costa IDSB, Mamo T, Yemefack M, Aulang MS, Yagi K, Hong SY, Vijarnsorn P, Zhang GL (2015) Status of the world's soil resources: main report. Embrapa Solos-Livro científico (ALICE). FAO website, downloaded on December 2021 from https://www.fao.org/documents/card/en/c/c6814873-efc3-41db-b7d3-2081a10ede50/
Nguyen KA, Liou YA, Tran HP et al (2020) Soil salinity assessment by using near-infrared channel and Vegetation Soil Salinity Index derived from Landsat 8 OLI data: a case study in the Tra Vinh Province, Mekong Delta, Vietnam. Prog Earth Planet Sci 7:1. https://doi.org/10.1186/s40645-019-0311-0
Paredes-Hernandez CU, Salinas-Castillo WE, Guevara-Cortina F, Martinez-Becerra X (2013) Horizontal positional accuracy of Google Earth's imagery over rural areas: a study case in Tamaulipas, Mexico. Boletim De Ciências Geodésicas 19:588–601. https://doi.org/10.1590/S1982-21702013000400005
Parida AK, Jha B (2010) Salt tolerance mechanisms in mangroves: a review. Trees 24(2):199–217
Scudiero E, Skaggs TH, Corwin DL (2015) Regional-scale soil salinity assessment using Landsat ETM+ canopy reflectance. Remote Sens Environ 169:335–343
Silva TS, Costa MP, Melack JM, Novo EM (2008) Remote sensing of aquatic vegetation: theory and applications. Environ Monit Assess 140(1):131–145
Silvestri S, Marani M (2004) Salt-marsh vegetation and morphology: basic physiology, modelling and remote sensing observations. Ecogeomorphol Tidal Marshes Coast Estuar Stud 59:5–25
Tilley DR, Ahmed M, Son JH, Badrinarayanan H (2007) Hyperspectral reflectance response of fresh water macrophytes to salinity in a brackish subtropical marsh. J Environ Qual 36:780–789
USGS (2022) Landsat Collection 2. Online at: https://www.usgs.gov/landsat-missions/landsat-collection-2. Accessed Jan 2022
Vargas R, Pankova EI, Balyuk SA, Krasilnikov PV, Khasankhanova GM (2018) Handbook for saline soil management. FAO/LMSU. Downloaded on

December 2021 from https://www.fao.org/documents/card/en/c/I7318EN/
Wang DONG, Poss JA, Donovan TJ, Shannon MC, Lesch SM (2002) Biophysical properties and biomass production of elephant grass under saline conditions. J Arid Environ 52(4):447–456
Wassmann R, Phong ND, Tho TQ, Hoanh CT, Khoi NH, Hien NX, Vo TBT, Tuong TP (2019) High-resolution mapping of flood and salinity risks for rice production in the Vietnamese Mekong Delta. Field Crop Res 236:111–120
Yu L, Gong P (2012) Google Earth as a virtual globe tool for Earth science applications at the global scale: progress and perspectives. Int J Remote Sens 33(12):3966–3986
Zhang TT, Zeng SL, Gao Y, Ouyang ZT, Li B, Fang CM, Zhao B (2011) Using hyperspectral vegetation indices as a proxy to monitor soil salinity. Ecol Indic 11(6):1552–1562
Zhang TT, Qi JG, Gao Y, Ouyang ZT, Zeng SL, Zhao B (2015) Detecting soil salinity with MODIS time series VI data. Ecol Ind 52:480–489

Publisher's Note